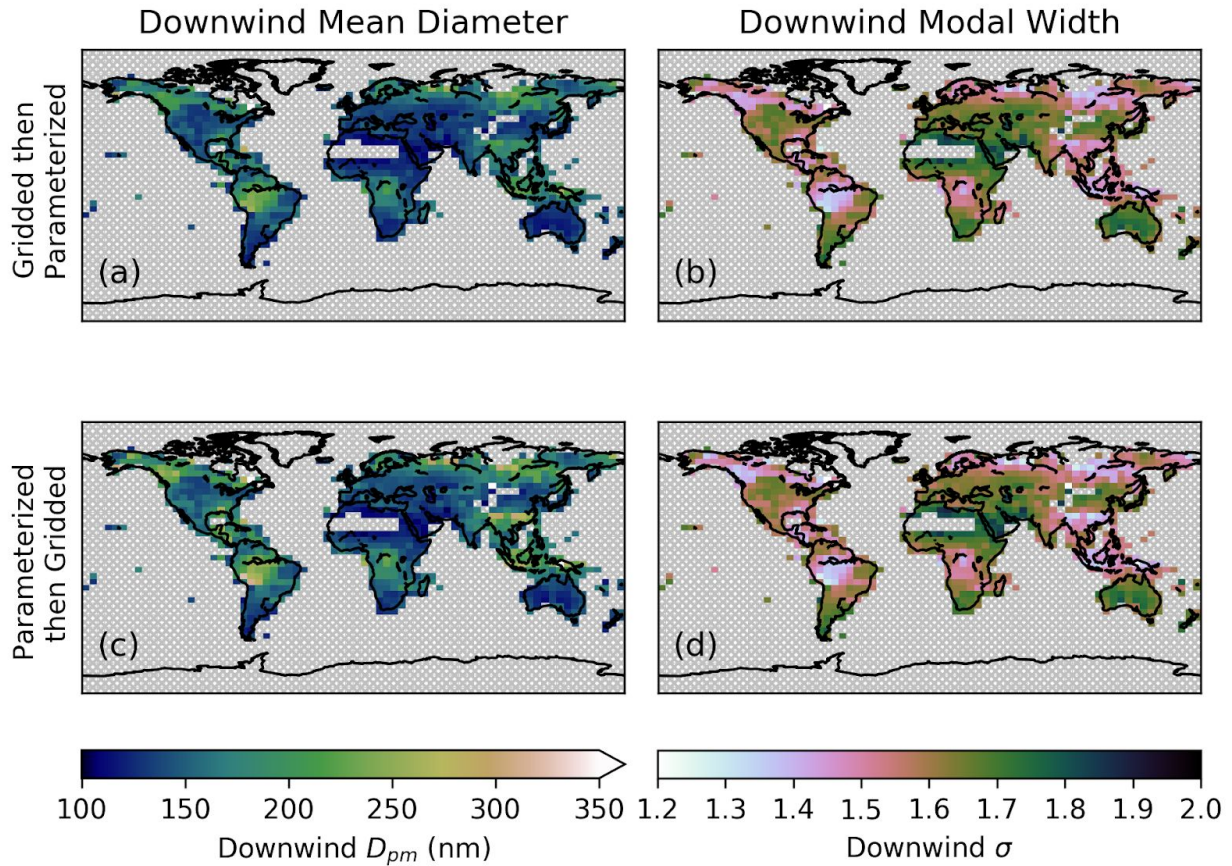
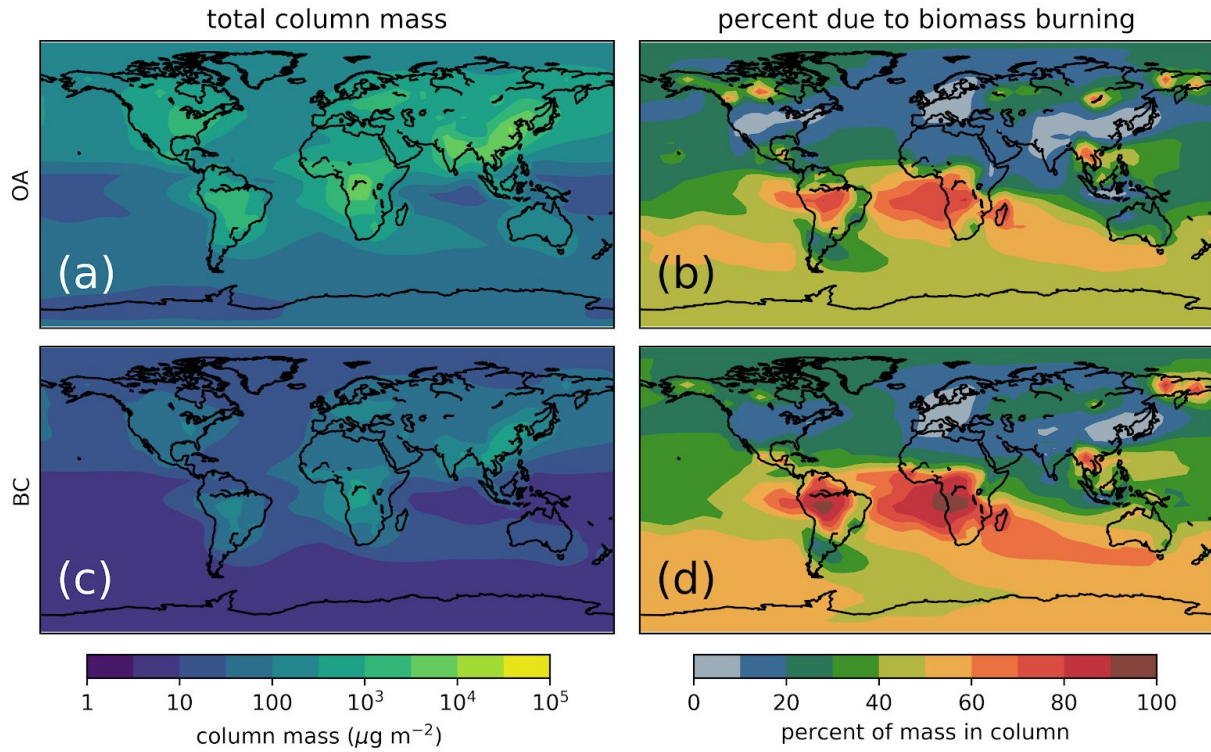


**Figure S1: Demonstration of the effect of per-fire coagulation parameterization on all the fires in the Western US on 8/15/2015 from FINNv1.5.** The emissions of OA and BC are indicated in the color in (a) and in the size of the markers in (b) and (c). In (a) the size indicated the area of the fire. In (b) and (c) the color indicates the median diameter and modal width, respectively, after 24 hours of coagulation where the emitted median diameter is 100 nm and the emitted modal width is 2.



**Figure S2: Annual-mean median diameter (a and, c) and modal width (b and, d) for biomass burning emissions predicted for 2010 using the Sakamoto et al. (2016) parameterization after 24 hours of sub-grid coagulation with an emitted initial median diameter of 100 nm and an emitted initial modal width of 2. Panels (a) and (b) show the resulting  $D_{pm}$  and  $\sigma$  when the fire (FINNv1.5) and meteorological data is averaged over a  $4^\circ \times 5^\circ$  grid and then that gridded data is run through the Sakamoto et al. (2016) parameterization. Panels (c) and (d) show the results when the individual fires are run through the Sakamoto et al. (2016) parameterization and then the output  $D_{pm}$  and  $\sigma$  are averaged over a  $4^\circ \times 5^\circ$  grid. The regions with grey cross-hatching are grid-cells with no fire data.**



**Figure S3: Effect of biomass burning on annually averaged total column OA and BC mass concentrations. The left side shows the total column mass concentration of (a) OA and (c) BC in the simulations with FINNv1 biomass burning emissions (i.e., *noSubCoag\_FINN*). The right side shows the percent of the mass in the column that is due to biomass burning emissions for (b) OA and (d) BC by taking the difference between the *noSubCoag\_FINN* and *noBB* simulations.**

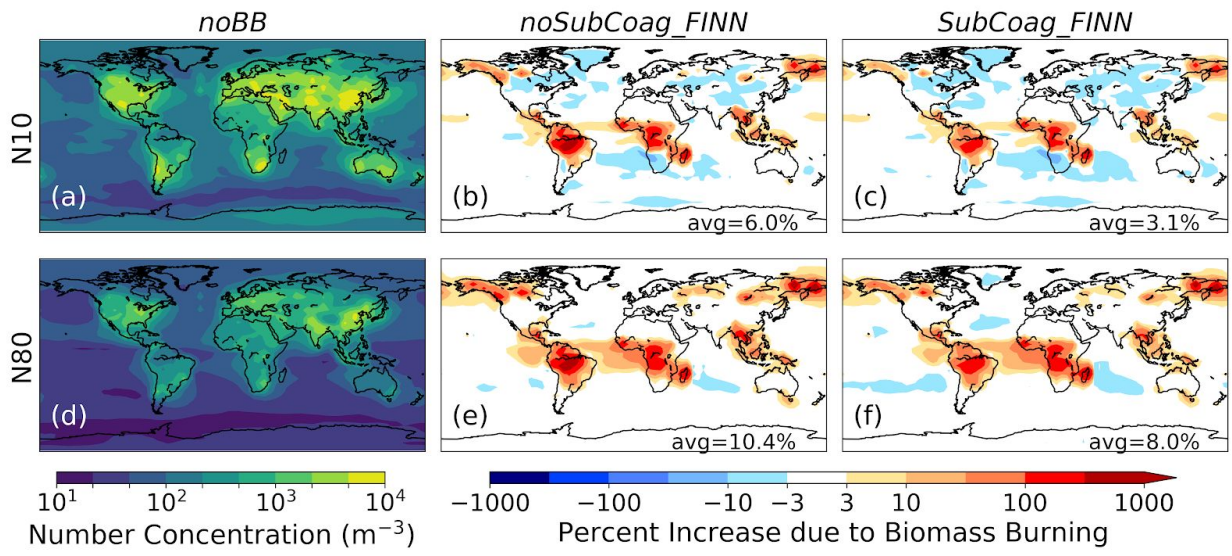


**Figure S4: Effect of biomass burning on surface-level number concentration of particles above 10 nm (a, b, c) and 80 nm (d, e, f).** Panels (a) and (d) show the absolute number concentration for the *noBB* simulation. Panels (b) and (e) show the percent increase due to FINNv1 biomass burning emissions from the *noBB* simulation to the *noSubCoag\_FINN* simulation. Panels (c) and (f) show the percent increase due to FINNv1 biomass burning emissions from the *noBB* simulation to the *SubCoag\_FINN* simulation. The number in the bottom right of each panel is the global mean percent increase due to biomass burning.

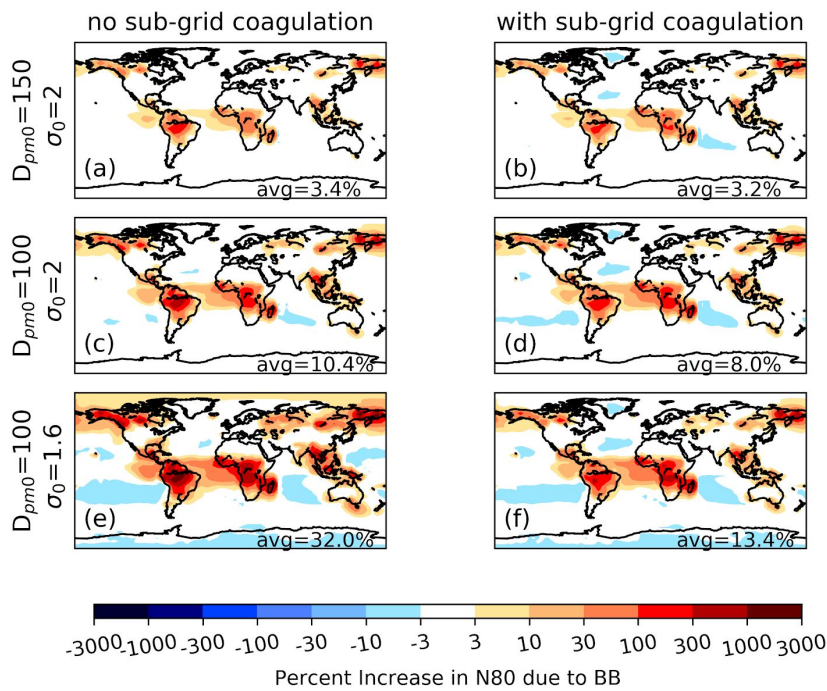


**Figure S5: Annual-average percent changes in N80 at the surface level due to the inclusion of FINNv1 biomass burning emissions relative to the simulation without biomass burning (*noBB*). Panels (a), (c), and (e) have no sub-grid coagulation (*D150\_noSubCoag\_FINN*, *noSubCoag\_FINN*, and *s1.6\_noSubCoag\_FINN*, respectively). Panels (b), (d), and (f) have sub-grid coagulation (*D150\_SubCoag\_FINN*, *SubCoag\_FINN*, and *s1.6\_SubCoag\_FINN*, respectively). Panels (a) and (b) have an emitted median diameter of 150 nm and an emitted modal width of 2. Panels (c) and (d) have an emitted median diameter of 100 nm and an emitted modal width of 2. Panels (e) and (f) have an emitted median diameter of 100 nm and an emitted modal width of 1.6. The number in the bottom right of each panel is the global mean percent increase in N80 due to biomass burning.**

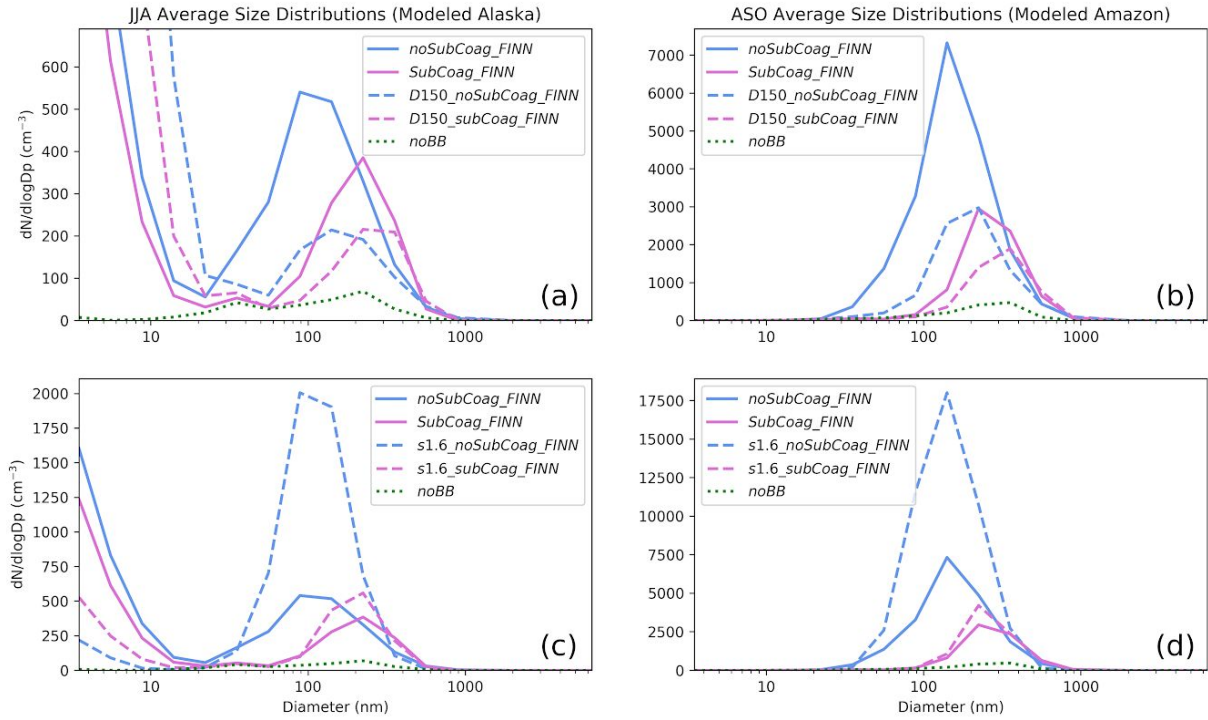


**Figure S6: Predicted grid-resolved aerosol size distributions with FINNv1 biomass burning emissions over Alaska at  $62^\circ$  N,  $140^\circ$  W, averaged over the June, July, and August fire season (a and c) and the Amazon at  $6^\circ$  S,  $60^\circ$  E, averaged over the August, September, and October fire season (b and d). All panels show the size distributions for the *noBB*, *noSubCoag\_FINN*, and *SubCoag\_FINN* simulations in the dashed green, solid blue, and solid pink lines, respectively. The top panels (a and b) show the sensitivity to the emitted median diameter, and the bottom panels (c and d) show the sensitivity to the emitted modal width. Note the different y-axis scales.**

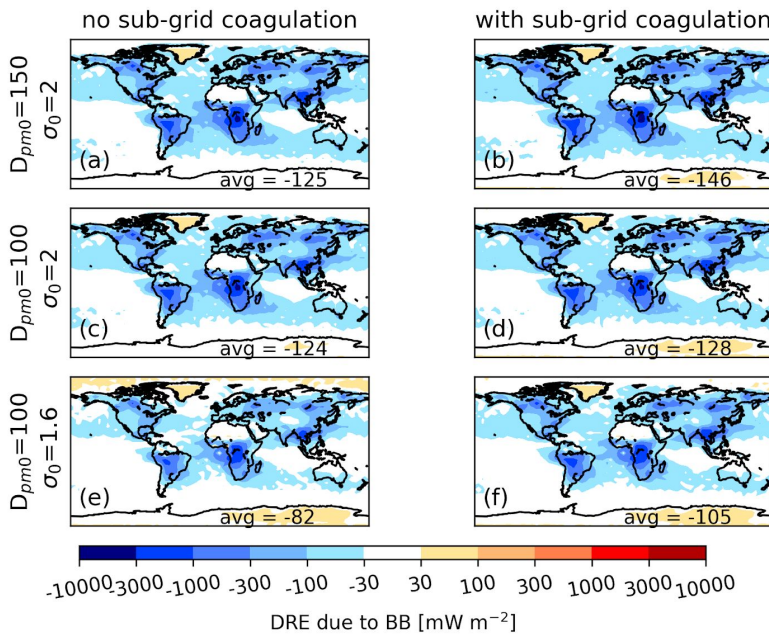


**Figure S7: All-sky direct radiative effect (DRE) due to biomass burning aerosols using FINNv1 emissions and using the external-mixing assumption. Panels (a), (c), and (e) are without sub-grid coagulation (`D150_noSubCoag_FINN`, `noSubCoag_FINN`, and `s1.6_noSubCoag_FINN`, respectively). Panels (b), (d), and (f) are with sub-grid coagulation (`D150_SubCoag_FINN`, `SubCoag_FINN`, and `s1.6_SubCoag_FINN`, respectively). Panels (a) and (b) have an emitted median diameter of 150 nm and an emitted modal width of 2. Panels (c) and (d) have an emitted median diameter of 100 nm and an emitted modal width of 2. Panels (e) and (f) have an emitted median diameter of 100 nm and an emitted modal width of 1.6. The number in the bottom right of each panel is the global mean DRE value [ $\text{mW m}^{-2}$ ].**

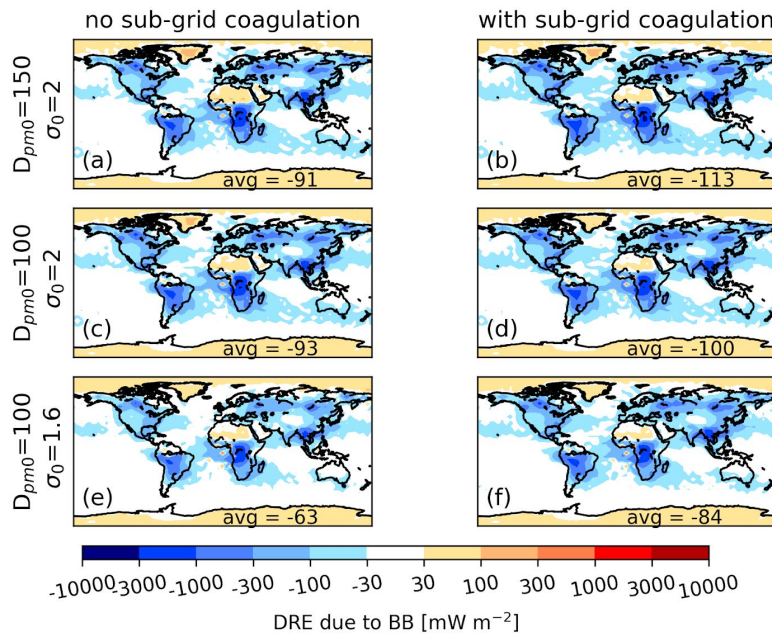


**Figure S8: All-sky direct radiative effect (DRE) due to biomass burning aerosols using FINNv1 emissions and using the core-shell mixing assumption. Panels (a), (c), and (e) are without sub-grid coagulation (*D150\_noSubCoag\_FINN*, *noSubCoag\_FINN*, and *s1.6\_noSubCoag\_FINN*, respectively). Panels (b), (d), and (f) are with sub-grid coagulation(*D150\_SubCoag\_FINN*, *SubCoag\_FINN*, and *s1.6\_SubCoag\_FINN*, respectively). Panels (a) and (b) have an emitted median diameter of 150 nm and an emitted modal width of 2. Panels (c) and (d) have an emitted median diameter of 100 nm and an emitted modal width of 2. Panels (e) and (f) have an emitted median diameter of 100 nm and an emitted modal width of 1.6. The number in the bottom right of each panel is the global mean DRE value [ $\text{mW m}^{-2}$ ].**

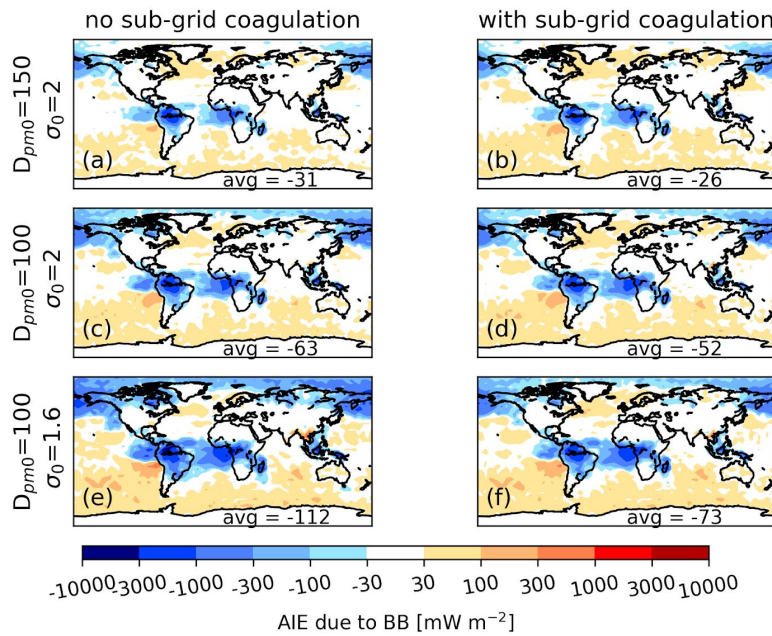


**Figure S9: Cloud-albedo aerosol indirect effect (AIE) due to biomass burning aerosols using FINNv1 emissions and using the external-mixing assumption. Panels (a), (c), and (e) are without sub-grid coagulation (*D150\_noSubCoag\_FINN*, *noSubCoag\_FINN*, and *s1.6\_noSubCoag\_FINN*, respectively). Panels (b), (d), and (f) are with sub-grid coagulation(*D150\_SubCoag\_FINN*, *SubCoag\_FINN*, and *s1.6\_SubCoag\_FINN*, respectively). Panels (a) and (b) have an emitted median diameter of 150 nm and an emitted modal width of 2. Panels (c) and (d) have an emitted median diameter of 100 nm and an emitted modal width of 2. Panels (e) and (f) have an emitted median diameter of 100 nm and an emitted modal width of 1.6. The number in the bottom right of each panel is the global mean AIE value [mW m<sup>-2</sup>].**

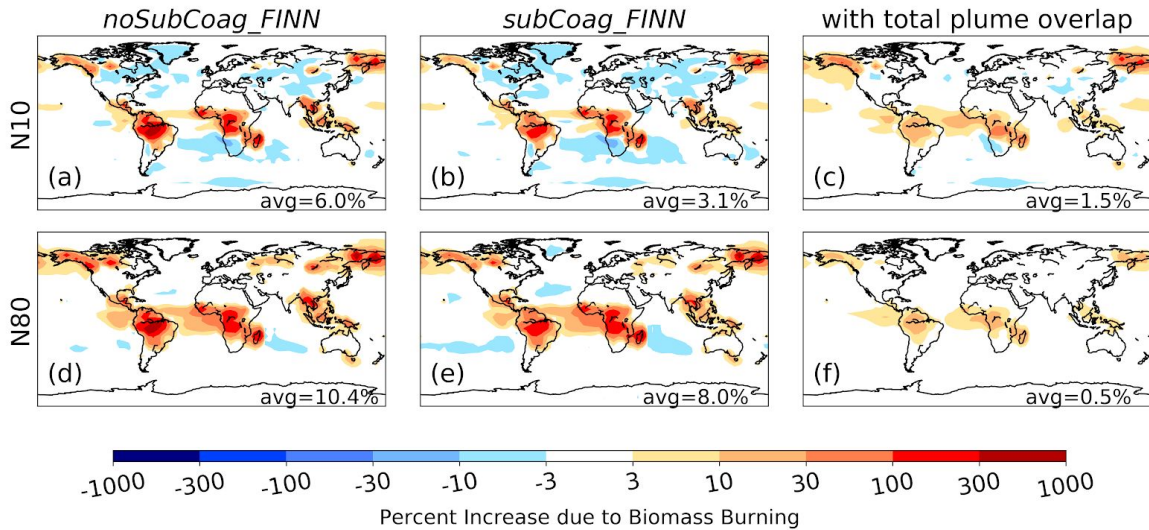


**Figure S10: Effect of biomass burning on surface-level (from 1013 hPa to 998 hPa) N10 (a-c) and N80 (d-f) under three sub-grid coagulation conditions. Panels (a) and (d) show the *noSubCoag\_FINN* case (no sub-grid coagulation). Panels (b) and (e) show the *SubCoag\_FINN* case (with sub-grid coagulation as in the rest of the paper, where the smoke plumes are treated as without overlap). Panels (c) and (f) show a new case where all smoke plumes in the gridbox completely overlap and form a single “superplume” upon emission into the sub-grid coagulation parameterization. All panels show the percent increase due to FINNv1 biomass burning emissions relative to the *noBB* simulation. The number in the bottom right of each panel is the global mean percent increase due to biomass burning.**

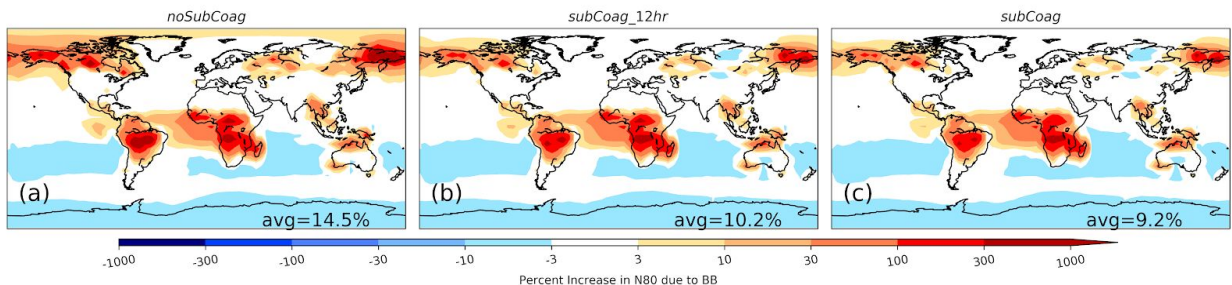


**Figure S11: Annual-average percent changes in N80 at the surface level (from 1013 hPa to 998 hPa) due to the inclusion of GFED biomass burning emissions relative to the simulation without biomass burning (*noBB*). On the left, there is no sub-grid coagulation (*noSubCoag*). In the middle, the sub-grid coagulation time is 12 hours (*SubCoag\_12h*). On the right, the sub-grid coagulation time is 24 hours (*SubCoag*). The number in the bottom right corner of each panel is the global mean percent increase in N80 due to biomass burning.**

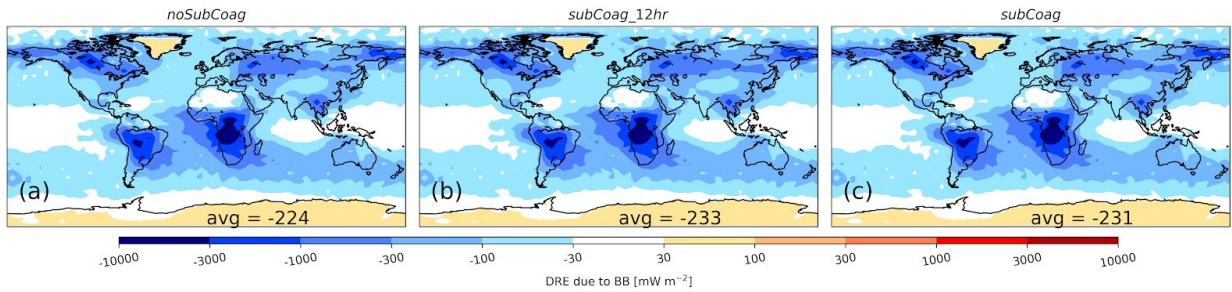


**Figure S12: All-sky direct radiative effect due to biomass burning aerosols using GFED emissions and the external-mixing assumption. On the left, there is no sub-grid coagulation (*noSubCoag*). In the middle, the sub-grid coagulation time is 12 hours (*SubCoag\_12h*). On the right, the sub-grid coagulation time is 24 hours (*SubCoag*). The number in the bottom right corner of each panel is the global mean value [ $\text{mW m}^{-2}$ ].**

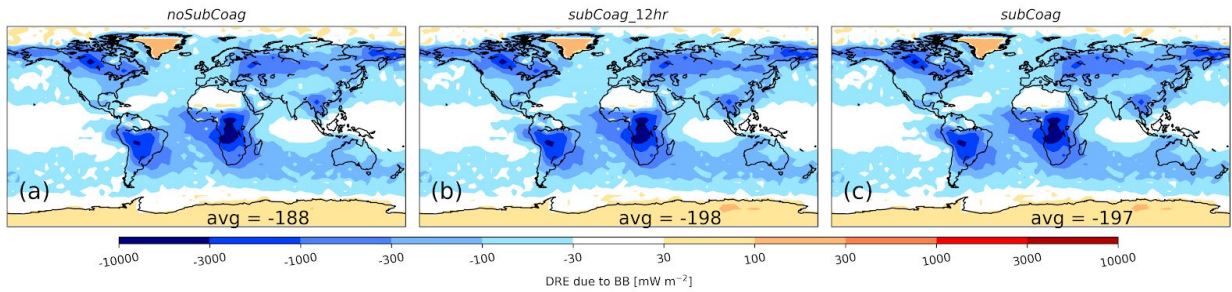


**Figure S13: All-sky direct radiative effect due to biomass burning aerosols using GFED emissions and the internal, core-shell mixing assumption. On the left, there is no sub-grid coagulation (*noSubCoag*). In the middle, the sub-grid coagulation time is 12 hours (*SubCoag\_12h*). On the right, the sub-grid coagulation time is 24 hours (*SubCoag*). The number in the bottom right corner of each panel is the global mean value [ $\text{mW m}^{-2}$ ].**

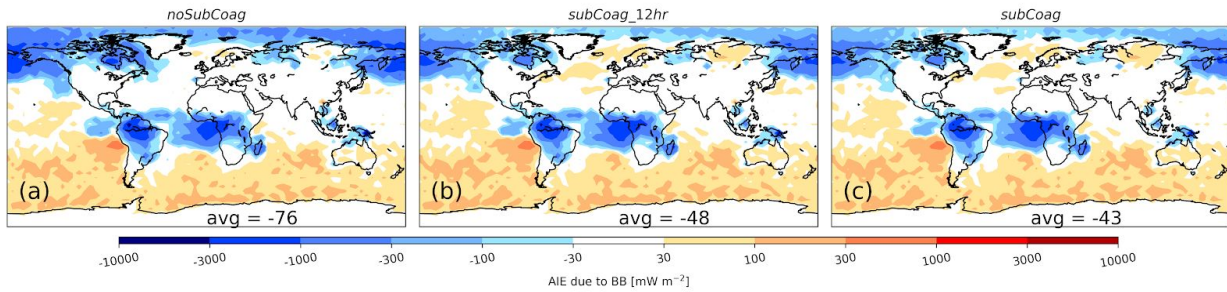


**Figure S14: Cloud-albedo aerosol indirect effect due to biomass burning aerosols using GFED emissions. On the left, there is no sub-grid coagulation (*noSubCoag*). In the middle, the sub-grid coagulation time is 12 hours (*SubCoag\_12h*). On the right, the sub-grid coagulation time is 24 hours (*SubCoag*). The number in the bottom right corner of each panel is the global mean value [ $\text{mW m}^{-2}$ ].**